Matter

CellPress

Article

Rapid tissue perfusion using sacrificial percolation of anisotropic networks

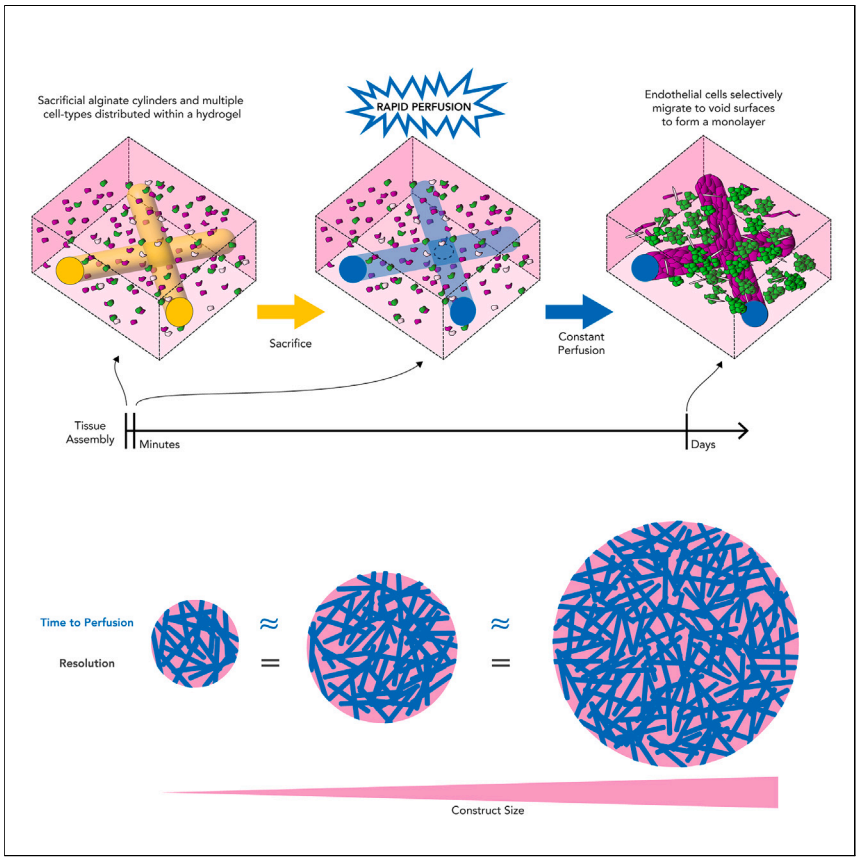

Tissue engineering has faced a persistent challenge to generate rapidly perfused microvascular networks at scale to support metabolic demands of resident cells. We overcome this challenge by developing a simple approach to create distributed percolated fluidic networks using sacrificial alginate cylinders. Perfusion is thereby achieved in minutes rather than hours, days, or weeks. We demonstrate the process in a wide variety of formats, along with vascularized liver and cardiac tissue constructs, highlighting its utility to a broad range of applications.

Alex Lammers, Heng-Hua Hsu, Subramanian Sundaram, ..., Yi-Chung Tung, Jeroen Eyckmans, Christopher S. Chen

chencs@bu.edu

Highlights

Scalable strategy that enables rapid perfusion of large, engineered tissues

Sacrificial anisotropic elements percolated to form a perfusion network

Pipettable process readily applicable to diverse manufacturing processes

Cell mixtures self-assemble into vascularized tissues

Demonstrate
Proof-of-concept of performance with intended application/response

Lammers et al., Matter 7, 2184–2204
June 5, 2024
https://doi.org/10.1016/j.matt.2024.04.001

CellPress

Matter

Article

Rapid tissue perfusion using sacrificial percolation of anisotropic networks

Alex Lammers,[1,2] Heng-Hua Hsu,[3] Subramanian Sundaram,[1,2] Keith A. Gagnon,[1] Sudong Kim,[1,2] Joshua H. Lee,[1] Yi-Chung Tung,[3] Jeroen Eyckmans,[1,2] and Christopher S. Chen[1,2,4,*]

SUMMARY

Tissue engineering has long sought to rapidly generate perfusable vascularized tissues with vessel sizes spanning those seen in humans. Current techniques such as biological 3D printing (top-down) and cellular self-assembly (bottom-up) are resource intensive and have not overcome the inherent tradeoff between vessel resolution and assembly time, limiting their utility and scalability for engineering tissues. We present a flexible and scalable technique termed SPAN (sacrificial percolation of anisotropic networks), where a network of perfusable channels is created throughout a tissue in minutes, irrespective of its size. Conduits with length scales spanning arterioles to capillaries are generated using pipettable alginate fibers that interconnect above a percolation density threshold and are then degraded within constructs of arbitrary size and shape. SPAN is readily used within common tissue engineering processes, can be used to generate endothelial cell-lined vasculature in a multi-cell type construct, and paves the way for rapid assembly of perfusable tissues.

INTRODUCTION

Efficient distributed mass transport is an indispensable prerequisite of life, enabling any cell within multicellular organisms to access necessary oxygen and nutrients in order to grow to sizes exceeding the diffusion limit.[1] To enable mass transport in highly metabolic tissues such as the liver, brain, and muscles, each cell in the tissue resides within ~200 μm of a capillary blood vessel.[2] When blood supply is interrupted, the tissue becomes ischemic within 20 min resulting in irreversible damage.[3]

Tissue engineers have long set out to create thick highly cellularized tissues for therapeutic applications. However, a major barrier to generate engineered tissue of clinically relevant size is the lack of a strategy to rapidly generate perfusable fluidic networks of appropriate caliber (10–150 μm diameter) throughout the tissue, while still operating in the temperature, pH, and aqueous confines dictated by living, cellularized tissues. Biological 3D printing has excelled at creating repeatable large-scale hollow structures (>200 μm),[4–8] including those with physiological cell densities,[9] but has yet to achieve the capillary scale networks required for effective tissue nutrient exchange. Light-based methods recently have achieved smaller length scales with high cell numbers,[6] but the serial nature of 3D printing nonetheless further increases assembly time as the vasculature becomes smaller and scale of the engineered tissue increases. In contrast, vasculogenic self-assembly can be employed to create capillary-sized structures (5–40 μm),[8,10–13] including from endothelial coated alginate beads.[14] However these methods take days to become

PROGRESS AND POTENTIAL

Despite 3 decades of significant progress in tissue engineering, a persistent challenge remains to generate rapidly perfusable vascular networks to support thick engineered tissues. We report a facile and scalable approach to rapidly assemble networks of hollow channels within cell-laden hydrogels and demonstrate its utility in generating high cell density engineered constructs.

Plastic dishes and bulk gel formats have long served as universal standards for 2D and 3D cell culture, and yet, despite being highly sought after, there is no such standard format for perfused cell culture in 3D gels. The fabrication strategy reported here is compatible with a wide range of established tissue engineering methods and cell culture in general. As such, the SPAN platform could be readily adopted as a standard approach to generating perfusable cultures of 3D tissues for both research and translational communities.

perfusable—too slow for highly metabolic tissues.[3] As a result, the rapid generation of appropriate-sized vasculature within large tissue constructs remains a significant challenge.

The problem of establishing rapid network connectivity through a material is not unique to vascular tissue engineering. In other fields, engineers and scientists have leveraged the advantage of anisotropic elements, including cylinders and spherocylinders, to model and rapidly create percolation networks for enhancing electrical conduction,[15–18] heat transfer,[19,20] mechanical reinforcement and structure,[21,22] and fluid flow[23–26] by allowing these elements to connect in an otherwise random distribution.

Here, we set out to investigate whether a percolation-based strategy could be used to rapidly generate a perfusable network to support tissue engineering applications. The system presented here, termed SPAN (sacrificial percolation of anisotropic networks), utilizes anisotropic alginate cylinders as pipettable sacrificial units that can be suspended into a bulk hydrogel prepolymer, spontaneously forming a percolated network. Following gelation of the surrounding material and degradation of the alginate fibers, a perfusable network of interconnected cylindrical voids is left behind by overlapping fibers. Furthermore, when the volume percentage occupied by the cylinders exceeds the percolation threshold, and reaches a percentage that establishes a distributed continuous network, perfusion can be circulated throughout a three-dimensional space rather than a single percolated fluidic path.[26–28] This technique is inherently scalable to arbitrary construct sizes and flexible to many applications. Here, we demonstrate that anisotropic sacrificial building blocks can be used to create unaligned percolated networks with established tissue engineering techniques such as needle casting,[13,29,30] suspended culture, and shear-aligned networks possible with 3D extrusion printing.[31–33] The process is compatible with a variety of hydrogels commonly used in cell culture. And finally, we apply this facile process to rapidly establish perfusion to support the function of dense, multi-cell-type laden constructs. In doing so, we further discover that the perfusable network guides tissue self-organization, whereby endothelial cells preferentially line the void surfaces while the stromal and parenchymal cells largely remain in the 3D matrix. The result is the generation of a perfusable vascularized network, all while maintaining perfusion across the entire tissue.

RESULTS

Microvascular-sized degradable fibers create a scalable fluidic network through percolation

We sought to develop a simple, robust system capable of rapidly establishing a perfusable fluidic network to support cells in various engineered tissues. To ensure broad applicability, this technique needs to be compatible with various hydrogel formulations and existing tissue engineering platforms. We chose alginate fibers as a sacrificial element due to their facile degradability and ease of mixing with various prehydrogel mixtures, both with and without cells. This combination could be dispensed to form a composite construct upon solidification, after which the alginate could be rapidly degraded to support perfusion. Although many scalable techniques exist to produce alginate fibers,[34–43] we opted to use only off-the-shelf materials for ease of adoption.

Our setup involved a standard syringe pump connected to a blunt-ended needle immersed in a spinning bath of calcium chloride to create fibers of different diameters ranging from of 10–150 μm (Figures 1Ai and S1). A quantification of

[1]The Biological Design Center and Department of Biomedical Engineering, Boston University, Boston, MA 02215, USA

[2]Wyss Institute for Biologically Inspired Engineering, Harvard University, Boston, MA 02115, USA

[3]Research Center for Applied Sciences, Academia Sinica, Taipei 11529, Taiwan

[4]Lead contact

*Correspondence: chencs@bu.edu

https://doi.org/10.1016/j.matt.2024.04.001

60 μm and 120 μm diameter fibers is shown in Figure S2. After crosslinking, the fibers were manually cut to specific lengths between 250 μm and 1 mm (Figure S1), sterilized, and stored in aliquots at high concentration until used. An expanded illustration of the process is shown in Figure S1 along with example needle sizes, pump speeds, and resulting fiber diameters shown in Table S1. Long-term storage in a microcentrifuge tube format allowed for the addition of various prehydrogel mixtures, with or without cells, using a standard wide-orifice pipette tip (as in Figure 1Aii) when desired. When the hydrogel is crosslinked, the embedded fibers become immobilized within the 3D construct (Figure 1Aiii). Example combinations of fiber diameters, lengths, and filler volumes crosslinked within a fibrin hydrogel are shown in Figure S3. Once the surrounding hydrogel is crosslinked, the fibers can be degraded either immediately or at a later time (Figure 1Aiv) to create a perfusable network with anisotropic voids in the shape of the sacrificial fibers.

Establishing a percolated network requires the fluidic integration of individual anisotropic voids. By introducing a calcium chelator such as ethylenediaminetetraacetic acid (EDTA) or alginate lyase (AL), an enzyme that rapidly degrades alginate, the contact area between two alginate fibers forms an open inter-vessel junction that connects the two remaining cylindrical voids in the gel (Figure 1B). The probability of these junctions fluidically connecting increases as the volume fraction of the fibers increases.[15,16,27,44] This is where the fluidic network becomes volumetrically dispersed to drive sufficient mass transport to support living tissue.

The true power of this process lies in its scalability to any construct size without compromising the resolution of the microvasculature. To demonstrate this advantage, we developed a water-in-oil emulsion system (Figure 1C) to produce large spherical hydrogels with embedded alginate fibers (Figure 1D). Since we only needed to pipette a larger volume of the mixture, fabricating hydrogels of different sizes took the same amount of time. AL was included at a concentration to drive fiber degradation in ~30 min, though increasing concentration would result in even faster time to completion. The agarose spheres, containing fibers that were 60 μm in diameter and 1 mm long, were crosslinked for 5 min and transferred to a well of PBS containing 20 mM EDTA for 15 min. Then, the spheres were perfused with 500 nm fluorescent beads for 15 min, fixed, and cut into 500 μm sections. Confocal images of the middle sections show that the voids were filled with fluorescent beads, suggesting that the spheres were successfully perfused through the voids (Figures 1E and S4).

Compatibility of SPAN with current tissue fabrication techniques and biomaterials

Next, we explored the compatibility of SPAN with well-established formats for generating engineered tissues, now with perfusable vasculature throughout the constructs. Using a common fiber/matrix prepolymer of 1% w/v agarose as the bulk gel, we successfully generated spheroid droplet cultures now with enhanced perfusion in orbital shaker culture baths (Figure 2A); constructs formed within a PDMS fluidic device could be perfused within the device (Figure 2B), with a 1-cm construct shown in Figure S5; shear-aligned network constructs were made by flowing the composite material through a channel before polymerization (Figure 2C); and a construct connected to a larger microfluidic lumen was made by sacrificially casting the composite material around acupuncture needles (Figure 2D). A temporally color-coded image of 6 μm beads flowing from the needle cast channel to the fiber-created void is shown in Figure S6.

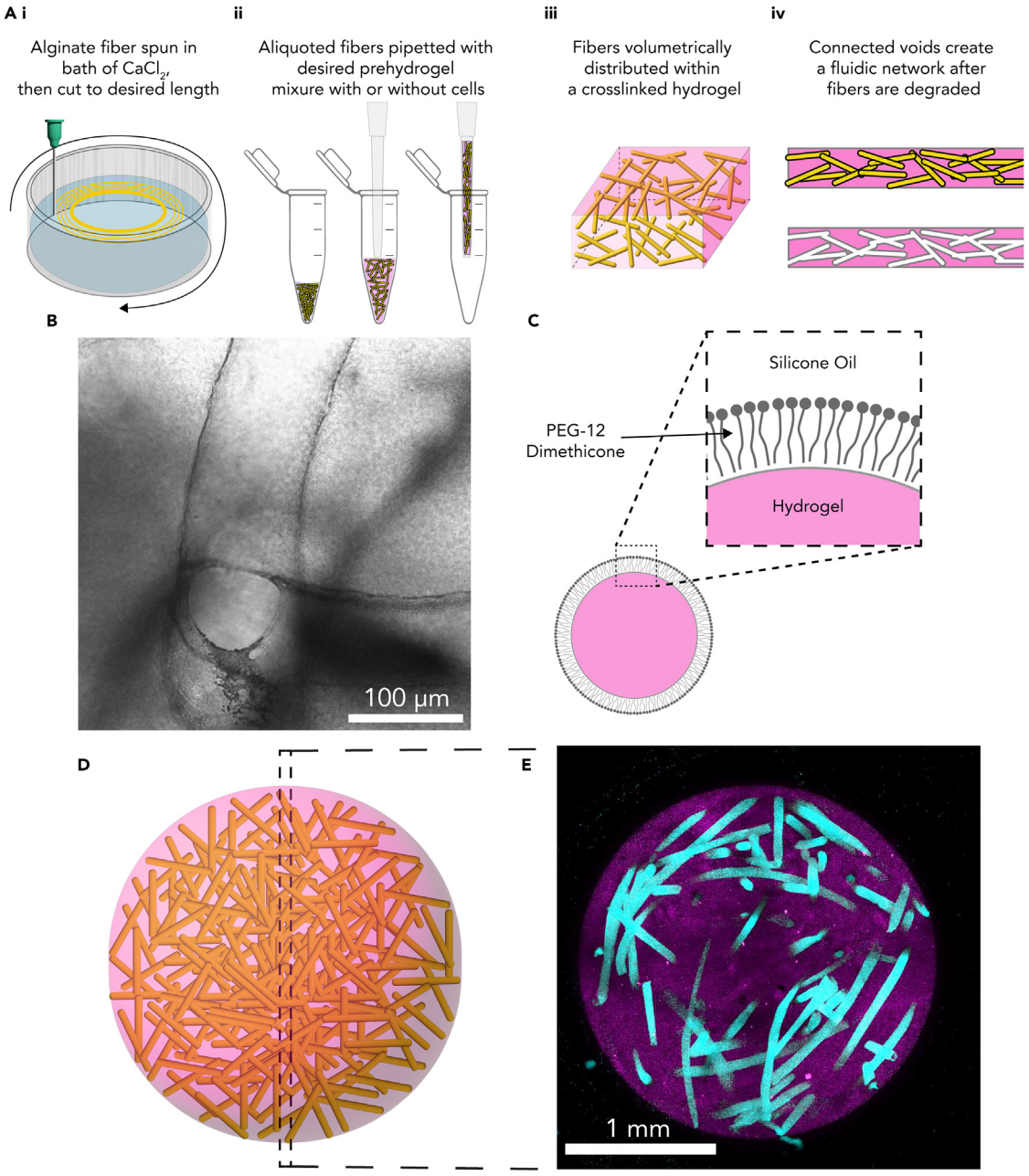

Figure 1. Microvascular-sized degradable fibers create scalable fluidic network through percolation

(A) Schematic depicting the fabrication of fibers and the pipettable percolation technique.

(B) Brightfield image of an inter-vessel junction in a fibrin hydrogel after the alginate has been degraded. Fibrin was stained with Crystal Violet to enhance contrast.

(C) Cartoon showing the water-in-oil emulsion technique used to fabricate large hydrogel spheres.

(D) Rendering of spherical hydrogel encapsulating alginate fibers that can selectively be degraded when desired.

(E) Max projection of middle 500 μm section of 2.5 mm spherical agarose gel, with beads embedded in gel (magenta), after degradation and external perfusion of beads through the intact sphere (cyan). See also Figures S1–S4.

To assess the versatility of SPAN with other materials, we cast gels made of agarose, collagen, or fibrin with embedded alginate fibers into a fluidic PDMS device (Figure 2E) and degraded the alginate fibers prior to perfusion with fluorescent beads. The fluorescent beads were found throughout the percolated networks in physically

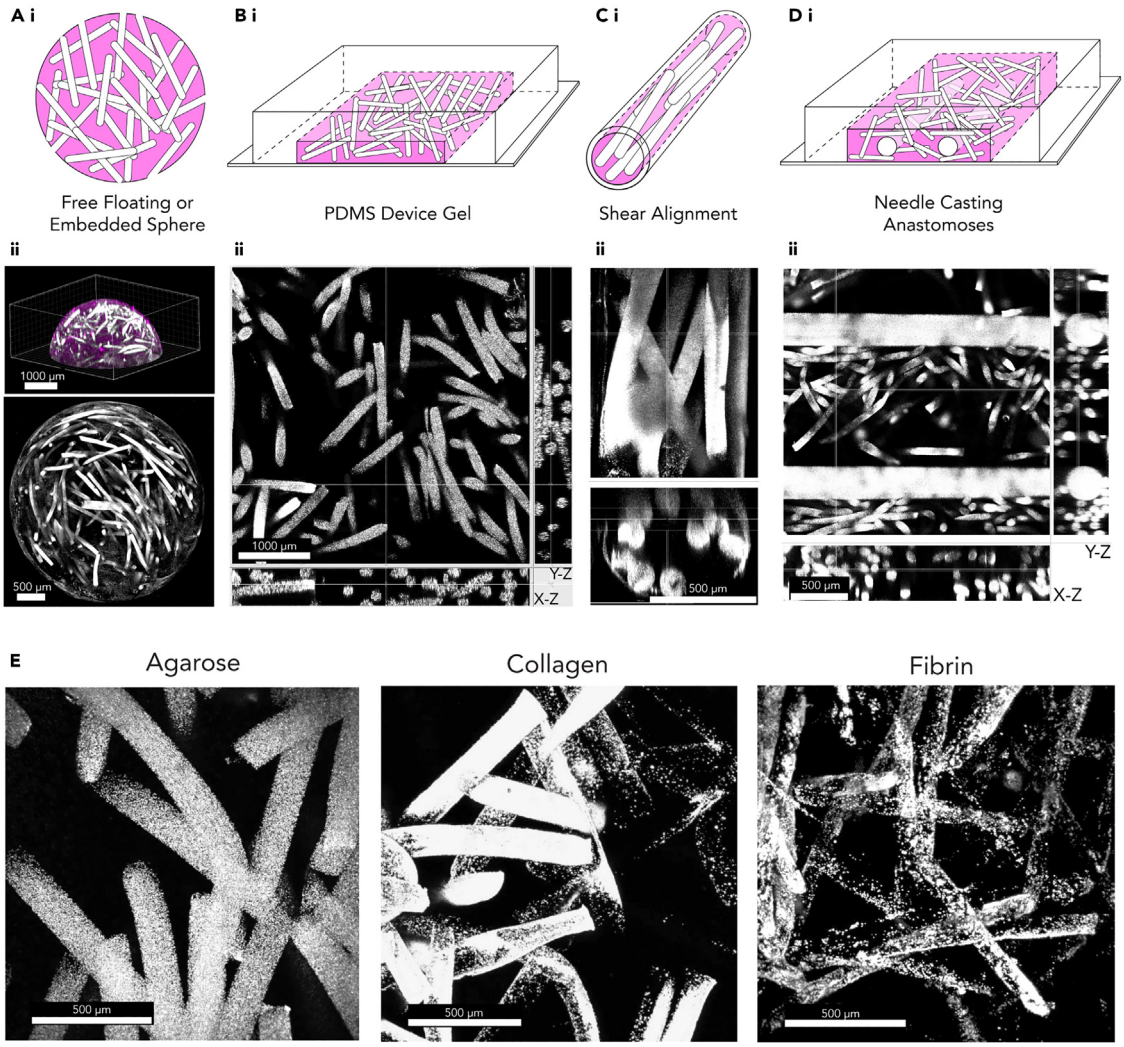

Figure 2. Rapidly patterning percolated networks with existing tissue engineering techniques and materials

(Ai) Rendering showing perfused network within a spherical gel and (Aii) below showing a projected image of magenta beads embedded within an agarose hydrogel show the spherical shape and perfused beads show the connected fluidic network (white), with bottom image showing a max projection from above.

(Bi) Rendering of PDMS fluidic device and (Bii) showing a cross-section image of agarose gel with perfused voids (white) showing the dispersed and three-dimensional distribution of the network.

(Ci) Illustration of the ability of anisotropic elements to shear align within a confined structure with (Cii) showing a cross-section of perfused voids (white) in an agarose hydrogel that are aligned within the confines of 750 μm diameter tubing.

(Di) Rendering of a microfluidic device with two large cylindrical channels fabricated by using acupuncture needles to mold fluidic channels in an agarose hydrogel with alginate fibers pipetted along with a pre-hydrogel gel mixture into a gel port. After needles were removed and alginate fibers degraded, the needle channels were fluidically connected throughout the bulk agarose gel with a cross-section image shown in (Dii).

(E) Cross-sections of perfused voids (white) within commonly used hydrogels including agarose, collagen, and fibrin. (Aii top and Bii) Scale bars, 1 mm; (Aii bottom, Cii, Dii, and E) scale bars, 500 μm. See also Figures S5 and S6.

(agarose, collagen) and enzymatically (fibrin) crosslinked gels, irrespective of whether they are uniform bulk gels or fibrous in nature. Collectively, these findings show that SPAN is compatible with various tissue fabrication techniques and natural materials without the need to further optimize the construct formulation.

SPAN enhances mass transport to support living cells within a construct

To investigate our platform's ability to achieve adequate oxygen/mass transport to cells and prevent cell death, we systematically varied the fiber cylinder parameters,

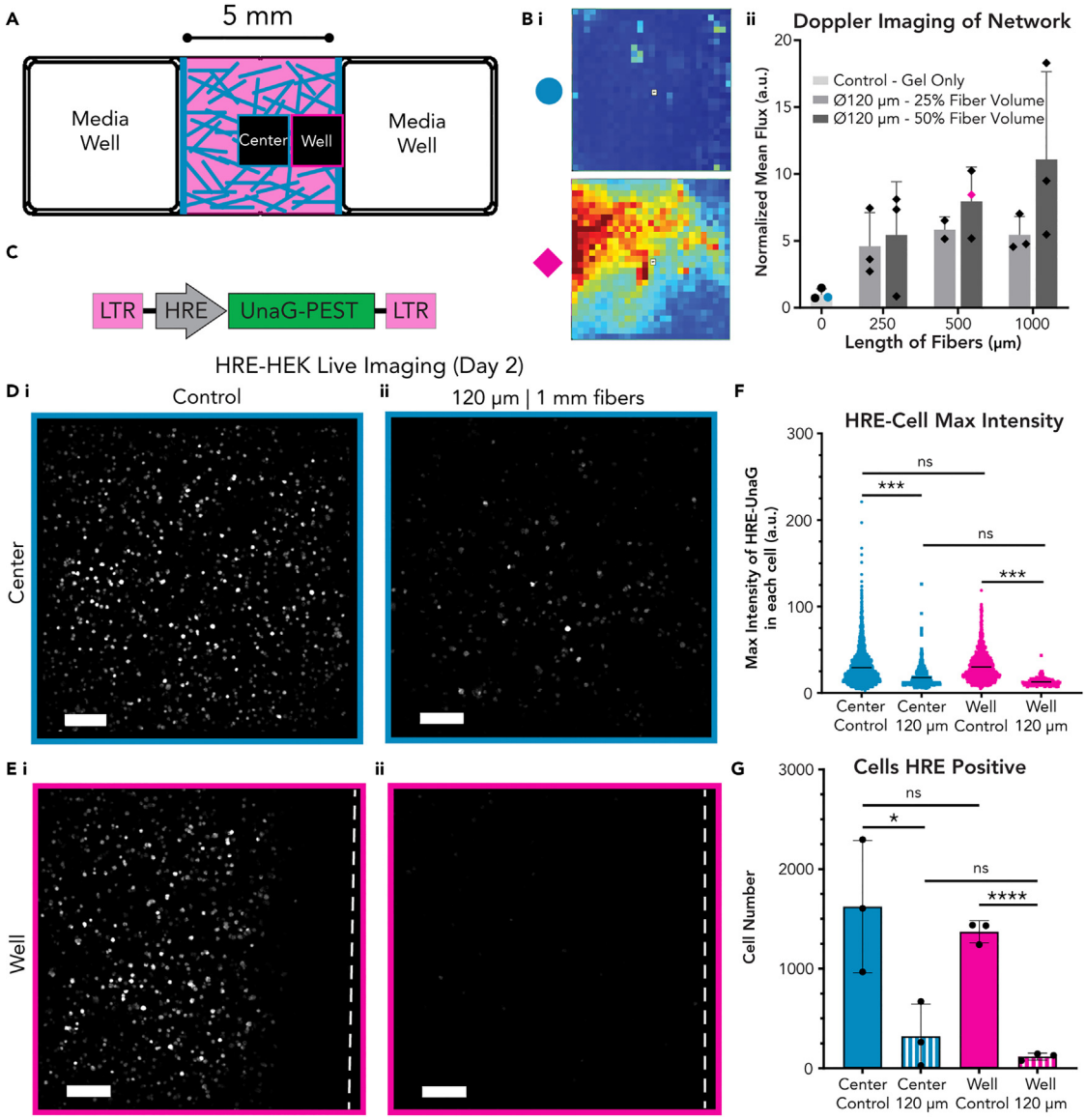

Figure 3. Percolated perfusion significantly reduces hypoxia within tissues

(A) Schematic of PDMS device with a 5 × 5-mm gel region that is 750 µm in height. Two areas were imaged: the center of the gel (blue box) and near the media well (magenta box).

(Bi) Representative Doppler flux images of a fibrin only gel (top, blue circle) and a percolated network (bottom, magenta diamond), shown in quantification of normalized mean fluid flux with varied parameters (Bii).

(C) Diagram of a hypoxia sensor used to assess mass transport with individual cells.

(D and E) Max projections of HEK293 cells (25 M/mL conc.) expressing the hypoxia sensor in control (Di and Ei) and void (Dii and Eii) gels. Edge of media well shown as dotted white line (Ei and Eii).

(F) Quantified violin plot of max intensity of the HRE fluorescence in individual cells and (G) the cell numbers expressing HRE fluorescence in each device. Data are represented as mean ± SEM. ****: $p \leq 0.0001$, ***: $p \leq 0.001$, *: $p \leq 0.05$ ns = not significant. Scale bars, 200 µm. See also Figures S7 and S8.

including filler volumes (25%–50%), fiber lengths (250 µm–1 mm), and fiber diameters (60–120 µm) within fibrin gels in a fluidic PDMS device, represented in Figure 3A. Although we explored the use of fibers up to 2 mm long, we constrained our maximum length to 1 mm to maintain uniform pipettability of the pre-gel solution using a standard wide-orifice pipette tip. For fibers 120 µm in diameter, we achieved

consistent percolation using a filler volume of 25%, a percentage reminiscent of vasculature volume percentages observed in cell-dense *in vivo* tissues (15%–30%).[45–48] However, Doppler imaging, used to assess the fluid flux through the gel after degradation of the alginate fibers, revealed enhanced fluid flux through the construct in an enclosed device (Figures 2B and 3A) when the filler volume was increased to 50% (Figure 3B). Furthermore, while shorter fibers have the advantage of more compact packing within a volume, computational models have shown that the advantage of this increased density is outweighed by the necessity for fluidic connections to be established between each void within the system.[25,44] Consistent with these predictions, the longest pipettable cylinder unit (1 mm) provided us with the largest average fluid flux among the tested fibrin gels. Given that the highest mean flux was achieved using 120 μm diameter fibers that were 1 mm long at a filler volume of 50%, we used this condition to determine if the increased mass transport provided by the perfused network was sufficient to prevent hypoxia within dense, cell-laden engineered tissue constructs, a common surrogate used to infer adequate oxygen delivery to the tissue.[49]

To test the ability of the percolation networks to support viable tissue, we utilized a hypoxia reporter that was originally developed for investigating hypoxia in tumor models.[50,51] Briefly, this construct couples UnaG, an eel fluorophore with a chromophore capable of oxygen-independent maturation, to a PEST degron, which ensures rapid degradation of any low-level leak in the circuit and enables detection of transient changes in degree of oxygenation (Figure 3C). This fluorescent reporter is driven by a minimum CMV promoter and five hypoxia response elements (HRE), such that cellular stabilization of native HIF1 in hypoxic environments drives construct expression. Under normoxic conditions, the fluorescent protein is minimally expressed, while under hypoxic conditions (∼<5% oxygen) the UnaG protein accumulates within the cytoplasm of the cell.[50,51] Using this construct, we established and calibrated (Figure S7), a HEK293FT-HRE cell line to detect hypoxia in our tissue constructs.

HEK293 cells rapidly degrade fibrin gels,[52,53] therefore we embedded HEK-HREs, at a 25 million cells/mL concentration, into collagen gels with or without alginate fibers that measured 120 μm in diameter and 1 mm in length at a 50% filler volume. These constructs were cultured for 2 days on a standard cell culture rocker to drive fluid flow, and live-cell imaging was conducted in two different areas, shown in Figure 3A, with a blue square showing the "center" region and a magenta square showing the "well" region. This allowed us to assess the hypoxia at the periphery near the source of cell culture media and in the very center of the device.

While the bulk collagen gels enabled adequate mass transport to allow HEKs to survive, they exhibited significant hypoxia in both the center gel region (Figure 3Di) and media well region (Figure 3Ei) except for the strip within ∼300 μm of the media well itself. In contrast, the gels interspersed with the percolated fluidic networks showed significantly reduced hypoxia as measured by a decrease in the maximum intensity of the hypoxia reporter signal in individual cells (Figure 3F) and the lower number of HRE-positive cells (Figure 3G) compared with control gels. We observed some variance in levels of hypoxia in samples prepared under identical conditions, and upon closer examination found that the density of fibers, and therefore perfusion, can vary locally (Figure S8). Thus, while SPAN enables rapid tissue assembly and supports much-needed mass transport, it can leave some portions of a tissue underperfused.

Endothelial cell-lined vessel networks generated with SPAN

Engineered tissues not only necessitate a fluidic network to sustain them but also demand a functional vasculature lined with an endothelial cell monolayer to provide active regulation of transport between vessel lumens and the tissue.[54] Traditional tissue engineering approaches have often relied on introducing endothelial cells into a construct via an inlet channel to coat fabricated channels. This approach has proven effective in printed luminal structures (~200 μm–1 mm) compared with the diameter of endothelial cells in suspension (~20–50 μm). However, as conduits decrease in diameter closer to those of individual cells, complete lumen occlusion can become more frequent as multiple cells can jam into a narrowing passage. Moreover, a highly distributed network is difficult to uniformly coat, especially when the fluidic junction between voids is smaller than the diameter of the individual voids themselves, as was the case with our networks.

Rather than introducing endothelial cells through an inlet channel to populate the percolated networks, we sought to leverage the natural propensity of endothelial cells to line and populate lumens. We hypothesized that by simply distributing endothelial cells in the bulk gel, they would find and populate the existing perfused network, without interfering with the ability to perfuse the constructs throughout (Figure 4A). To assess the feasibility of this approach, we employed the large format device from Figure 3A (5 × 5 × 0.75 mm^3 hydrogel). Fibrin hydrogels containing human microvascular endothelial cells (HMVECs; 2 M/mL) were formed with or without alginate fibers. The devices containing only HMVECs in fibrin were unable to establish a perfused network (Figure 4Bi). Despite the presence of some multicellular structures, seen in Figures 4Bii–4Biv and Video S1, no large lumenized network could be found. In contrast, perfused networks consisting of either 60 μm (Figure 4Ci) or 120 μm voids (Figure 4Di) that were 1-mm long and made up less than 25% of the tissue volume, became preferentially lined with endothelial cells over the course of several days, with continuous perfusion being supported during the entire period of study (Figures 4C and 4D). To gain deeper insights into how the endothelial cells interacted with the voids and gels, we captured high-magnification images of the fibrin gel using reflectance microscopy, along with F-actin of the endothelial cells in the center of each device (Figures 4Biii, 4Ciii, and 4Diii). While the endothelial cells did not fully cover the exposed fibrin within the voids, analysis of the entire construct for three repeats of each fiber condition revealed that 73% of the 60 μm voids were covered in an endothelialized monolayer and 51% of the 120 μm voids were covered (Figure S9). Importantly, the inter-vessel junctions between 60 μm and 120 μm voids remained intact and fully endothelialized (Figures 4Civ and 4Div, Videos S2 and S3). These findings suggest that the surface created after the cylinder degradation is a preferential substrate for HMVECs to cover without the need of specialized growth factors or support cells.

SPAN supports perfusion and organization of an endothelialized vasculature within engineered tissues

Although the assembly of an endothelialized fluidic network is useful for certain applications, we sought to investigate the feasibility of applying this approach in the presence of stromal and parenchymal cells. Our initial focus involved creating an engineered construct modeling liver tissue. To achieve this, we incorporated HepG2 cells, an immortalized hepatocyte line, primary human dermal fibroblasts as stromal cells (HDFs), and primary human umbilical vein endothelial cells (HUVECs) into our constructs. Similar to our previous experiments, the cells were uniformly distributed within the constructs and cultured for 5 days (Figures 5A and 5C). Control constructs over that period either lacking alginate fibers (Figures 5B and S10A, Video S4) or

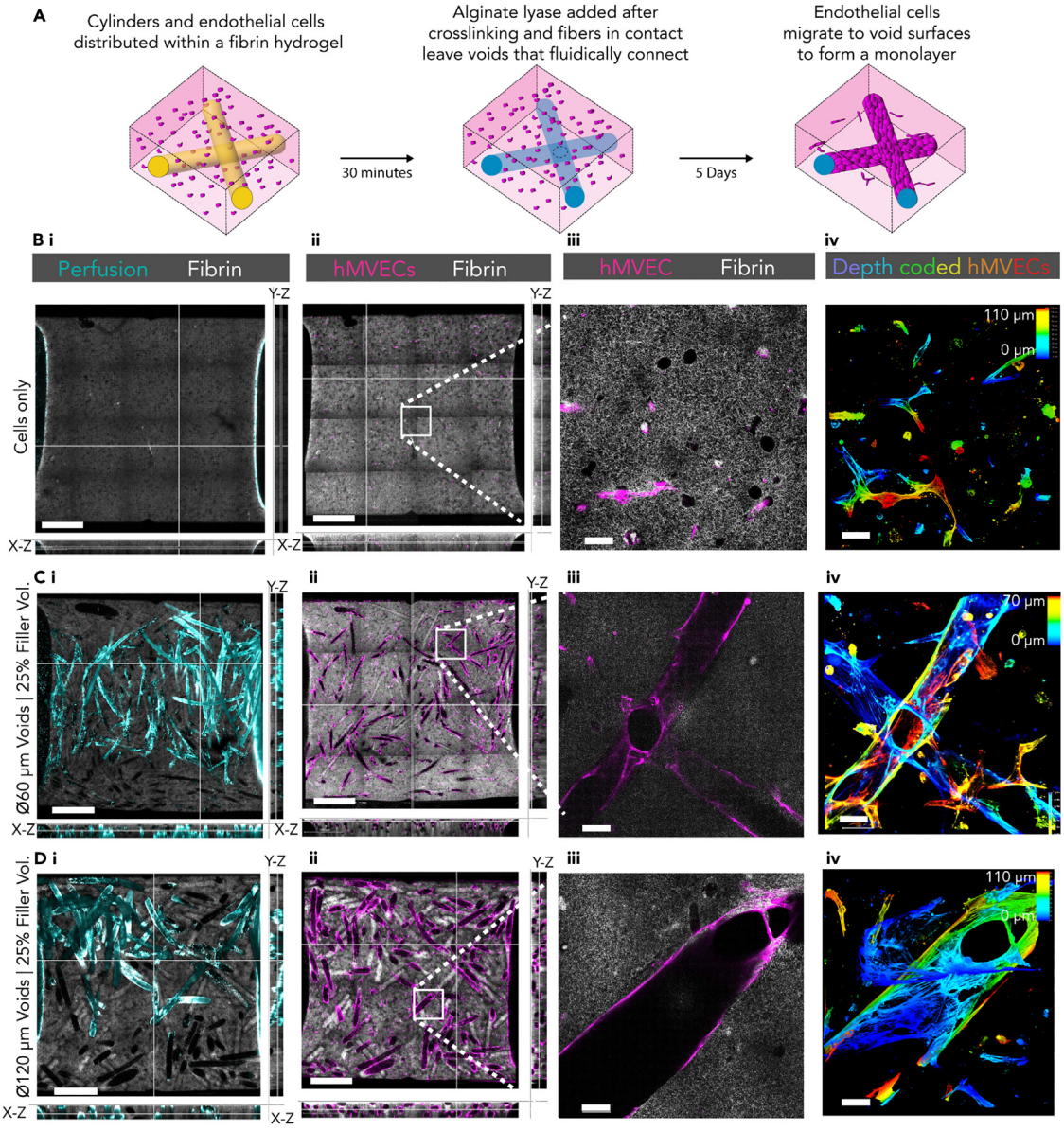

Figure 4. Endothelialization of voids from cells embedded in hydrogel after 5 days

(A) Schematic of hydrogel formation, perfusion, and endothelialization.

(Bi, Ci, and Di) Images of cell only control and void devices. Extended cross-sectional images of perfusion (cyan) fibrin gel (white).

(Bii, Cii, and Dii) Extended cross-sections of same devices with of hMVEC Endothelial cells (magenta).

(Biii, Ciii, and Diii) Zoomed in optical slice of devices. (Biv, Civ, and Div) Depth coded max projections of same area as (iii).

(B, C, Di, and Dii) Scale bars, 1 mm; (B, C, and Diii–iv) scale bars, 50 µm. See also Figure S9 and Videos S1, S2, and S3.

lacking endothelial cells (Figure S11B) showed the HepG2 cells and fibroblasts still preferred remaining in the bulk gel. Conversely, tissue constructs with percolated networks were largely lined by endothelial cells, while the HepG2 cells and fibroblasts remained in the gel (Figures 5D and S10B, Video S5).

To further demonstrate generalizability of this approach to create perfused parenchymal tissue, we replicated the assembly process to model heart tissue (Figures 5E and 5G). In this iteration, we substituted hepatocytes with inducible pluripotent cell-derived cardiomyocytes and monitored the constructs over a shorter period

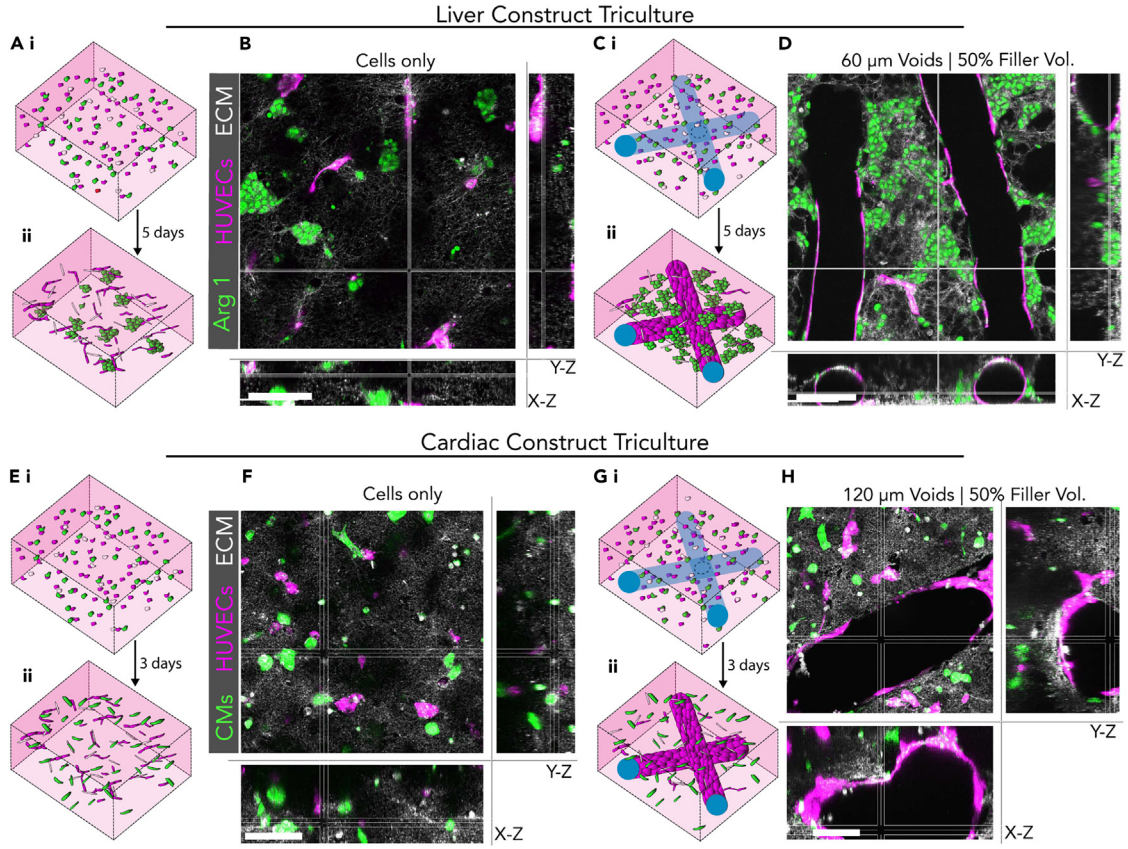

Figure 5. Endothelial cells preferential coat voids in presence of other cell types

(A and C) Schematics of cell only (A) and perfused SPAN (C) remodeling liver construct tricultures at seeding (i) and 5 days later (ii).

(B and D) Extended cross-sections of day 5 HepG2s+HDFs+HUVECs triculture control, and fiber tissues, respectively.

(E and G) Schematics of cell only (E) and perfused SPAN (G) remodeling cardiac construct tricultures at seeding (i) and 5 days later (ii).

(F and H) Extended cross-sections of day 3 CMs + HDFs + HUVECs triculture control, and fiber tissues, respectively. Scale bars, 100 μm. See also Figures S10 and S11 and Videos S4 and S5.

(3 days). Similar to the liver constructs, we observed that endothelial cells lined the perfused networks while the cardiomyocytes and fibroblasts remained in the bulk (Figures 5H and S10D), while the constructs without percolated networks did not even form lumenized structures (Figures 5F and S10C). Cardiac conditions without HUVECs similarly resulted in cells remaining in the bulk gel (Figure S11D). Collectively, these data suggest that SPAN facilitates the rapid assembly of constructs that not only support the perfusion requirements for engineered tissues, but also provide architectural cues enabling endothelial cells to form a vasculature in the presence of stromal and parenchymal cell populations.

DISCUSSION

The generation of large-volume tissue constructs has been limited by a lack of approaches to generate a perfusable vasculature required to provide adequate transport of nutrients and oxygen to cells throughout the construct.[1,2,55] Recent advances in 3D printing have demonstrated the possibility of generating perfusable networks with arbitrary architectures but are thus far limited to larger (>200 μm diameter) lumens, still an order of magnitude larger than those of natural tissues (<10 μm).[4–6,8,9,56–58] Because transport efficiency is limited by the surface area for diffusion between vascular lumens and the bulk tissue, smaller and

more dense vessel networks are needed.[2,55] While laser-induced degradation of materials can generate smaller lumens[8,59] and further improvements in 3D printing could eventually achieve the desired resolutions,[8] these serial fabrication strategies in general cannot escape the tradeoff between resolution and build time. For the assembly of cellularly dense living tissues, rapid perfusion is required to avoid tissue necrosis and failure.[3] Here, we have demonstrated a pipettable one-pot, two-step approach—percolated assembly and dissolution—that requires a fixed time (minutes) to achieve construction and perfusion, irrespective of construct size. These distinct and controllable steps allow for fiber degradation timing to be tuned to the specific bulk material used. The pipettability of the SPAN system also allows access to many enclosed systems used in tissue engineering such as microfluidic devices and bioreactors that are otherwise inaccessible to 3D printers, along with standard tissue culture formats such as 96-well plates. And while we only focused on lumen diameters spanning the range between those available through either vasculogenic self-assembly or 3D printing, others have used a microfluidic device to create pure alginate fibers with diameters down to ~2 μm,[35] and electrospun down to 90 nm.[60] The simple approach presented in this paper could address the long-recognized need for generating perfusable constructs of arbitrary size.

Using this approach, we demonstrated the ability to generate and adequately perfuse constructs densely packed with cells. It has previously been demonstrated that the diffusion distance of oxygen in native tissues can range from 200 to 500 μm.[2,55] Here, we observed a similar diffusion distance when cells incorporating a hypoxia-sensitive reporter were densely packed (~25 million cells/mL) in a solid gel. In contrast, hypoxia was relieved in SPAN gels, where the density of perfused networks was sufficient to deliver oxygen throughout the network. Given the general compatibility of this approach to develop percolated networks in a variety of forms, biomaterials, and fabrication processes, we anticipate that SPAN could be applied to a wide range of tissue engineering applications.

In addition to rapidly constructing paths for perfusion within a construct, we demonstrated that SPAN can be used to generate engineered vascular networks lined with endothelial cells. The primary approach currently to build living vascular networks is through a process of vasculogenic self-assembly[12,13,61–63] where endothelial cells distributed in a bulk gel are able to spontaneously find each other, form an interconnected network of cells, and then degrade the gel within their vicinity to form a dense perfusable vascular network. Alternatively, *in vivo* studies have shown that the presence of microvascular scale channels within a gelatin hydrogel is sufficient to rescue ischemic injury through host angiogenesis.[64] However, these processes take days to weeks, and are not compatible with the requirements to perfuse newly assembled constructs quickly. By seeding the endothelial cells into the bulk of gels, we observed that when they encounter the SPAN-generated network of voids, they preferentially exit the bulk gel to line the inner surface of the voids, rapidly generating a scalably endothelializable network of lumens. Because the density of voids is designed to be high (for perfusing the construct), endothelial cells in the bulk appear to encounter the voids quickly and assemble the vasculature within days. However, unlike self-assembly approaches that require time-consuming cell-mediated tissue vascularization, the entire SPAN construct is perfused within minutes of assembly such that the tissue is adequately supported while the endothelial cells seek and line the voids to form a functional vasculature. Demonstrating that this strategy to generate vascularized lumens can be used to build liver and cardiac tissues in minutes further highlights the potential utility of the approach. Thus, this

simple approach of incorporating SPAN upon construct assembly provides a pathway to engineering rapidly perfused large-scale engineered tissues.

Conclusions

In this work, we presented a novel tissue engineering platform, SPAN, that allows for rapid assembly of a perfusable vessel network in arbitrarily shaped and sized engineered tissues. The process consists of alginate fibers distributed in an arbitrary bulk material at sufficient densities to form an interconnected percolated network, which are then degraded to create a perfusable fluidic network throughout the construct. The relatively low volume taken up by the fluidic network allows for a large percentage of the construct to be filled with the engineered cell-containing tissue that can remodel and self-organize. Additionally, while this pipettable, one-pot technique can be used alone, its power comes from its compatibility with many existing tissue engineering processes, including automated liquid handling, 3D printing, microfluidic casting, vasculogenic self-assembly, and others. In summary, SPAN provides a flexible and simple system to overcome transport limitations in large-volume constructs and paves the way for rapid manufacturing of thick perfusable engineered tissues.

EXPERIMENTAL PROCEDURES

Resource availability

Lead contact

Requests for further information and resources should be directed to the lead contact, Christopher S. Chen (chencs@bu.edu).

Materials availability

No unique materials or reagents were generated in this study.

Data and code availability

All data are available within the main or supplementary texts or from the lead contact upon reasonable request. This study did not generate code.

Hydrogel fabrication

Fabrication, storage, and degradation of alginate fibers

Alginate fiber cylinders were fabricated and used as shown in Figure 1A and elaborated on further within Table S1 and Figure S1.

Fiber fabrication. Low-viscosity alginic acid sodium salt from brown algae (Sigma A1112) was mixed with MiliQ water (MilliporeSigma Ultrapure Water Pure Water Purification System) at 2% w/v, heated to 60°C for 2 h, then left in 4°C overnight. Rehydrated alginate was used within 1 week. To fabricate fibers, alginate was drawn into a 2- to 5-mL syringe (Norm-Ject) and left to come to room temperature. The syringe was connected to EVA plastic tubing (1 mm ID) via Luer lock adapters (McMaster-Carr) with a blunt-ended needle connected to the end (McMaster-Carr/World Precision/BSTEAN). Various gauges were used to achieve desired alginate fiber diameters. Dispensing speed was determined by a syringe pump (Fisher Scientific). A crystallization dish (PYREX, 95-mm ID) was mounted on a vertical motor controlled by a Feather microcontroller and motor shield (Adafruit), filled with 20 g/L calcium chloride dihydrate (Sigma) and spun at a speed of ~150 revs/min. Once the dish was up to speed, the blunt needle was inserted (~1 cm from the dish wall) and the shear force from the gelation bath extruded the fiber. After fabrication, the fiber was left to sit in the gelation solution for at least 20 min before cutting and then transferred to a solution of 10 mM $CaCl_2$.

Cutting. The gelled alginate fiber coil was then laid perpendicularly to an array of razor blades (Gillette 7 O'clock super platinum) with fixed spacing determined by custom cut microscope slides or polyimide sheets (McMaster-Carr) that were held together with a stainless steel binder clip (McMaster-Carr 12755T82), and then cut by rolling a syringe along the individual blades. Once cut, large pieces of fiber and fibers annealed to each other from the cutting process were removed. Fibers were kept in 5 mM $CaCl_2$ in MilliQ water at 4°C until aliquoted.

Sterilization (if desired). $CaCl_2$ solution was aspirated using a 40 μm cell strainer (Falcon) placed on 50-mL conical tube and inverted. Sterile filtered EtOH with 5 mM $CaCl_2$ was added to resuspend the fibers and left overnight at 4°C. The EtOH was aspirated, and fibers were washed 3× with sterile filtered HEPES buffered saline (HBS) w/5 mM $CaCl_2$. HBS was adapted from a Cold Spring Harbor Protocol[65] by adding 5 mM $CaCl_2$ and without sodium bicarbonate or other non-HEPES buffers since they can chelate calcium from ionically crosslinked alginate.

Aliquoting. Dilute cut alginate fibers were pipetted into open-ended 1 mL serological pipettes (Fisher Scientific 03-395-168) and left to settle out at the bottom of the pipette tip. After settling for ~30 min, fixed volumes of concentrated fibers were dispensed into 1.5 mL microcentrifuge tubes; 12.5-μL and 25-μL aliquots were most used. Aliquots were stored at 4°C and wrapped in parafilm to prevent evaporation until used. When mixing pre-gel solutions, use large orifice pipette tips any time pipetting fibers (USA Scientific #1011–8400).

Degradation. Alginate lyase (AL) (Sigma, A1603) was used in all studies requiring degradation of alginate. This enzyme is specific to the degradation of alginate, specifically M-block sugars, while not affecting cell viability over long periods of time. EDTA was used in addition to AL in the spherical gel demonstration to maximize degradation. While EDTA is a more commonly used reagent to decrosslink alginate gels, prolonged exposure of EDTA is lethal to cells.

Additionally, because the AL acts enzymatically, it can be included in the prehydrogel mix to slow enzymatic activity, and only when the temperature is raised to 37°C does the enzyme (evenly distributed throughout the construct) efficiently act to degrade the alginate.

Additional notes

Filler volumes. Twenty-five percent to 50% filler volumes were demonstrated in this report for largely practical considerations. Filler volumes ranging between 25% and 50% were able to facilitate the creation of disperse fluid flows while retaining the bulk gel structure within commonly used soft hydrogels, while leaving adequate volume to include bulk hydrogel precursors and high numbers of cells. Filler volumes of up to 75% were used, however, at this proportion some hydrogels (i.e., 2.5 mg/mL fibrin) begin to fail due to the resulting weak structure after degradation. However, increasing the stiffness and weight percentage of the bulk gel allows for high filler volumes. Additionally, pipetting mixture using filler volumes above 75% becomes difficult and resulting gels become inconsistent.

Fidelity. Void fidelity relative to the sacrificial alginate fibers is highly dependent on choice of bulk gel. Fibrin stress relaxes after crosslinking[66] and voids were found to expand ~5 μm after 12 h post crosslinking and degradation. In contrast, no detectable difference was found within 1% agarose between fiber and void diameters after degradation.

Tissue stability. The experiments presented in this paper involving tissue constructs were performed for a maximum of 5 days. However, with the same material system in a similar device with an increased number of fibroblasts, tissues appeared stable for 2 weeks without issue. However, without cells added, the many hydrogels presented can be stored for months at 4°C.

Agarose gel

(10 mg/mL final): Low gelling temperature agarose (Sigma A9414) was heated in HBS with 5 mM $CaCl_2$ until uniform. Agarose was then mixed with HBS w/5 mM $CaCl_2$ and alginate fibers then immediately put on ice to rapidly gel. For emulsion scaling study 500 μg/mL of AL was added last to other mixed prehydrogel components and then mixture was added immediately to oil emulsion.

Collagen gel

(5 mg/mL final): prepared as in Doyle,[67] except HBS with 5 mM $CaCl_2$ was used in place of DPBS++, and 10× low glucose DMEM came in liquid form (Sigma D2429). Briefly, Type I bovine collagen (Advanced BioMatrix TeloCol, 5226–9.8 mg/mL) was brought to a neutral pH on ice, then crosslinked for 1 h in a 37-°C tissue culture incubator with 5% CO_2, after which 500 μg/mL of AL was added overnight.

Fibrin gel

To make a fibrin gel at a final concentration of 5 mg/mL, fibrinogen (Sigma F8630 Lot # SLBS1440V) and thrombin (1 U/mL, Sigma T4648) solutions were made by first mixing HBS with $CaCl_2$ with the fibrinogen to neutralize the sodium citrate in the rehydrated fibrinogen, to prevent premature degradation of the alginate fibers. HBS with 5 mM $CaCl_2$, alginate fibers, and finally thrombin was then added. After the addition of thrombin, the solution was quickly injected into the tissue chamber, and the devices were repeatedly rotated over ~1 min while the solution crosslinked to ensure even distribution of alginate fibers.

Emulsion

Silicone oil AR20 (Sigma 10836) was mixed with PEG-12 Dimethicone (DOW, DOWSIL OFX-5329) with the emulsifier making up just 0.01% v/v. Aqueous gel solutions were pipetted directly into the solution and left to gel. A pre-gel mixture was then pipetted directly into the emulsion solution contained in a standard tissue culture plate. After the hydrogel crosslinks, it is then moved to a buffered solution or cell media.

Fluidic PDMS device assembly and treatment

The molds for the fluidic devices were constructed using stereolithography (Proto Labs). PDMS devices were fabricated and surface treated as described previously.[13] PDMS was cured at a standard 1:10 mixing ratio overnight at 60°C in the mold, and individual devices were cut and plasma-bonded to glass slides. To enhance ECM bonding to PDMS, the surface inside the tissue chamber of the devices was functionalized with 0.01% poly-L-lysine and 1% glutaraldehyde following plasma activation and washed overnight in DI water. On the day of seeding, devices were soaked in 70% ethanol (EtOH) and dried. Devices were UV-sterilized for 15 min before cell seeding.

Perfusion

Bead perfusion for imaging

Agarose gels were perfused with 500 nm fluorescent beads (Life Technologies F8812), while collagen and fibrin gels were perfused with 2 μm fluorescent beads (Polysciences – Fluoresbrite 19508-2) and either imaged during perfusion or fixed in place by photocrosslinking dextran-MA (86 kDa) mixed with the beads.

Doppler flux imaging

PDMS fluidic devices (5 mm × 5 mm × 0.75 mm) were fabricated, and surface treated as described above; 5 mg/mL fibrin gels were assembled encapsulating alginate fibers of varying length, and filler volume. Fibers were degraded and 2% milk (Hood) was perfused overnight at 4°C. The following day, devices were imaged with a Laser Doppler Imager (moorLDI2-IR, Moor Instruments) with a pressure head difference between wells of 9.25 mmH_2O.

Cell studies

Cell culture

HEK-293FT cells (Thermo Fisher Scientific R700-07, used before passage 10) were cultured in 1× DMEM (Corning) with 10% FBS (Gibco) and 1% Pen/Strep. Human dermal microvascular endothelial cells (hMVEC-Ds, Lonza) were cultured in EGM2-MV growth media (Lonza) and used at passages 4–7. Human dermal fibroblasts (HDFs, Lonza) were cultured in FGM-2 growth media (Lonza) and used at passages 4–7. HepG2 cells (ATCC) were cultured in EMEM (ATCC), with 10% FBS (ATCC), and 1% Pen/Strep. Human iPSC-derived cardiomyocytes were generated from the Harvard Personal Genome Project line 1 (PGP1, GM23338) (Seidman Lab at Harvard Medical School),[68] and were differentiated as in previous studies.[68,69]

Antibodies and reagents

DyLight 649 conjugated Anti-UEA I Lectin (Vector Laboratories, DL-1068-1) at a 1:500 dilution. Alexa Fluor 488/647 conjugated Phalloidin (Invitrogen/Thermo Fisher, #A12379/#A30107) and DAPI (Invitrogen/Thermo Fisher #D3571) were used at 1:1000 dilution. Anti-Arg1 (Atlas Antibodies, HPA003595) was used at 1:500 dilution followed with an Anti-rabbit secondary antibodies with Alexa Fluor Plus 647 (#A32733). Prior to cell staining, fixed tissues we blocked and permeabilized with 3% BSA.

Lentiviral transduction

Generation of HRE-HEK cells: 500,000 HEK293FT cells (Thermo Fisher Scientific R700-07, used before passage 10) were plated into a single well of a six-well plate. Twenty-four hours later, 1 μg of pLenti-HRE-dUnaG (gift from Roland Friedel, Addgene plasmid # 124372), 700 ng of pCMVR8.74 (gift from Didier Trono, Addgene plasmid # 22036), 200 ng of pMD2.G VSVG (a gift from Didier Trono, Addgene plasmid # 12259), and 100 ng of pAdVantage (Promega) were co-transfected into each well using an NaCl-polyethylenimine (PEI, 7.5 mM linear PEI stock, nitrogen/phosphorus ratio of 20, Polysciences) transfection. 72 h following transfection, supernatant was collected, filtered through at 0.45 μm filter, and concentrated using the PEG-IT viral precipitating agent (SBI). The viral pellet was then resuspended in 100 μL PBS and stored at −80°C. HEK 293 FT cells (passage 4) were plated in a six-well at a density of 100,000 cells per well. The next day, 50 μL of resuspended viral particles were added to each and allowed to incubate overnight. Media was changed 12 h after addition of viral particles. Forty-eight hours after viral transduction, cells were treated with media containing 1 μg/mL puromycin for 2 days. Cells that survived selection were tested for function (hypoxia-driven fluorophore expression and calibration (Figure S7)[70,71] and immediately cryopreserved.

LifeAct-Ruby-HUVECs were generated as in a previous study.[13] Briefly, HUVECs were transduced in growth media overnight with varying lentiviral titers that had been optimized for minimal changes in cell morphology and proliferation. The cells were then washed in PBS the next day and fed with fresh EGM-2 for expansion and then cryopreserved.

Hypoxia cell encapsulation and culture within collagen

On the day of device seeding, HRE-UnaG HEKs were growth arrested with 10 μg/mL mitomycin C (10 ng/mL final concentration) (EMD Millipore 475820) in DMEM growth media and washed five times in stock DMEM. HRE-HEKs were lifted from tissue culture plates using TrypLE Express (Gibco), centrifuged, and resuspended at a concentration of 250 million cells per mL in DMEM+. Cell-containing collagen hydrogels (2.5 mg/mL) were assembled as described above with HRE-UnaG HEKs (25 M/mL final concentration) and 1× DMEM+ added immediately after collagen solution was brought to a neutral pH.[67] The solution was then quickly injected into the tissue chamber, and the devices were manually flipped every 5 s for ~1 min while the solution crosslinked to ensure even distribution of the cells and alginate fibers. AL (250 μg/mL) was added 1 h after tissue assembly, placed on a programable rocker (Benchmark Roto-Bot) that paused for 3 min per side at angles of ±40° from level and left for 24 h. Media was exchanged daily.

Quantification of tissue hypoxia in vitro

After two days of culture, HRE-UnaG HEKs devices were live stained with Hoechst 33342 (ThermoFisher, H1399) at a 1:2000 dilution for 15 min. A pressure head was created between media wells to increase flow through the gel. Media was then exchanged from DMEM+ to L-15 Leibovitz media without phenol red (because the Leica microscope incubator did not have CO_2 capabilities and to reduce media autofluorescence). Images were captured according to the section "immunofluorescence and microscopy." Confocal stack images at 10× (for Figure 3) and 25× (for Figure S8) were captured and analyzed using built-in surface tools within Imaris 10.1.1 (Bitplane). For 10× and 25× images, surfaces were created surrounding individual cells within 3D stack using the thresholded fluorescence signal from HRE-HEK cells. The maximum intensity within individual cells was calculated along with the total number of cells expressing the HRE signal above a detectable threshold applied to all conditions.

Quantification of endothelial coverage

Confocal stack images of each tissue construct from the hMVEC encapsulation experiment were analyzed using ImageJ2[72] to determine the percent area coverage of the endothelial cells on the voids. Images were cropped to exclude the portions of the images that included the PDMS device and media wells. A sub-stack was created to exclude the image slices within the reflectance channel that showed reflection off the glass coverslip and slices where the endothelial signal was not robustly defined. Endothelial and reflectance channels were split into individual images and processed separately. A five-pixel median filter was applied to the reflectance channel slices, then a minimum projection was applied, followed by Huang auto thresholding.[73] A three-pixel median filter was applied to the endothelial channel, followed by sum projection and Huang auto thresholding. Respective endothelial and reflectance channels were then multiplied together, and the resulting image was compared with the reflectance min projection to ascertain a perfect area coverage of the endothelial cells within the fiber-created voids.

Endothelial cell and fiber encapsulation and culture within fibrin

HMVECs (2 M/mL final conc.) were encapsulated with or without alginate fibers (25% filler volume) in a 5 mg/mL fibrin gel as described above in "hydrogel fabrication." AL (250 μg/mL) was added 30 min after tissue assembly and left for 24 h. Devices were continually rocked on a cell culture rocker (Benchmark BenchRocker 2D) with tilt angles of 30° from level with daily media changes. After 5 days, devices were fixed, stained, and then imaged. False color was applied to both the UEA lectin,

Phalloidin, and 2 μm fluorescent polystyrene beads were false colored to magenta, magenta, and cyan, respectively.

Liver tissue model and fiber encapsulation and culture within fibrin

On the day of device seeding, HDFs were growth arrested with 10 μg/mL mitomycin C (10 ng/mL final concentration) (EMD Millipore 475820) in FGM-2 media and washed five times in FBM-2 basal media. HDFs, HepG2s, and LifeAct-ruby HUVECs were lifted from tissue culture plates using TrypLE Express (Gibco), centrifuged, and resuspended at a concentration of 20 M/mL in FGM-2 (HDFs), 50 M/mL in EMEM+ (HepG2s), or 100 M/mL in EGM-2 (HUVECs). Cells were then encapsulated with or without alginate fibers (50% filler volume) in a 5 mg/mL fibrin gel as described above in "hydrogel fabrication" at final concentrations of 1 M/mL (HDFs), 5 M/mL (HepG2s), and for the triculture condition – 10M/mL (HUVECs). Biculture tissues were cultured in EMEM+. Triculture tissues were cultured in a composite media consisting of ½ EMEM+ ½ EGM-2 with 2× growth factors and FBS, so that appropriate levels growth factors were available when the two media were mixed. AL (250 μg/mL) was added 30 min after tissue assembly and left for 24 h. Tissues were cultured for 5 days on a programmable rocker (Benchmark Roto-Bot) that paused for 3 min per side at angles of ±40° from level to drive flow through the gel between media wells. Media was changed daily. After 5 days the devices were fixed, stained, and then imaged by a Leica SP8 confocal microscope (Leica). False color was applied to the LifeAct-ruby, and Arg-1, and were false colored to magenta, and green, respectively.

Cardiac tissue model and fiber encapsulation and culture within fibrin and matrigel

On the day of device seeding, HDFs were growth arrested as elaborated above. HDFs, iPSC cardiomyocytes (iPSC-CMs), and and LifeAct-ruby HUVECs were lifted from tissue culture plates using TrypLE Express (Gibco), centrifuged, and resuspended at a concentration of 20 M/mL in FGM-2 (HDFs), 100 M/mL in RPMI+ (iPSC-CMs), or 100 M/mL in EGM-2 (HUVECs). Cells were encapsulated in a composite gel consisting of 5 mg/mL fibrin gel as described above in "hydrogel fabrication" and 10% Matrigel with final concentrations of 1 M/mL (HDFs), 5 M/mL (CMs), and for the tri culture condition - 10M/mL (HUVECs). Biculture tissues were cultured in a maintenance growth medium containing high-glucose Dulbecco's modified Eagle's medium (Thermo Fisher Scientific) supplemented with 10% fetal bovine serum (Sigma-Aldrich), 1% penicillin-streptomycin (Thermo Fisher Scientific), 1% nonessential amino acids (Thermo Fisher Scientific), 1% GlutaMAX (Thermo Fisher Scientific). Triculture tissues were cultured in a composite media consisting of ½ CM maintenance growth media +½ EGM-2 with 2× growth factors and FBS from both. 5 μM Y-27632, and aprotinin (0.016 mg/mL) were added to the media. The growth medium was replaced every day. Aprotinin was increased to 0.033 mg/mL after the first day. Y-27632 was removed 2 days following tissue seeding. Alginate lyase (250 μg/mL) was added 30 min after tissue assembly and left for 24 h. Tissues were cultured for 5 days on a programmable rocker (Benchmark Roto-Bot) that paused for 3 min per side at angles of ±40° from level. Media was changed daily. After 3 days (triculture) or 5 days (biculture) devices were fixed, stained, and then imaged by a Leica SP8 confocal microscope. False color was applied to the LifeAct-ruby, and GFP-titin, and were false colored to magenta, and green, respectively.

Immunofluorescence and microscopy

Brightfield images and fluorescent images (Figures 1B, S1, S3, and S7B) were acquired using a Nikon Eclipse TE200 epifluorescent microscope. All other images were captured using a Leica SP8 laser scanning confocal microscope (Leica) equipped with Leica 10×/0.30NA W U-V-I WD-3.60 Water and 25×/0.95NA W VISIR WD-2.50 Water objectives and Leica LAS X imaging software. For the live imaging

for the hypoxia study, the microscope incubator was preheated to 37°C and humidified. Within experimental runs, the laser intensities were kept constant, and the imaging settings were applied to all samples.

Image processing

Max projection and extended cross-section images used in figures were assembled and processed using Imaris 9.6.1 or 10.1.1 (Bitplane). Intensity of stack images was depth compensated by utilizing a built-in attenuation correction MATLAB plug-in (MathWorks).

Statistical analysis

All data are presented as mean ± standard deviation. At least three independent samples were analyzed for quantified sections. All statistical significance was determined using Prism 10.0 (GraphPad, San Diego, CA). Number of HRE-positive cells were quantified by unpaired two-tailed t tests. All other mean analyses were performed using ordinary one-way ANOVA and, where appropriate, followed by Tukey's honestly significant difference test to evaluate statistical significance (*$p \leq 0.05$, **$p \leq 0.01$, ***$p \leq 0.001$, and ****$p \leq 0.0001$).

SUPPLEMENTAL INFORMATION

Supplemental information can be found online at https://doi.org/10.1016/j.matt.2024.04.001.

ACKNOWLEDGMENTS

We would like to thank Linqing Li for having generated the dextran-MA material used in perfusion experiments. We also want to thank the Seidman Lab at Harvard Medical School for providing the iPSC-derived cardiomyocytes. This work was supported in part by grants from the NIBIB of the National Institutes of Health (R01 EB00262 and R01 EB033821), the National Science Foundation Engineering Research Center for Cellular Metamaterials (EEC-647837), the Paul G. Allen Frontiers Group Distinguished Investigator Program, and the Kilachand Multicellular Design Program. A.L. acknowledges support from the National Institutes of Health through the NHLBI (NIH F31 HL156517) and from the NIGMS T32 Quantitative Biology and Physiology training grant (NIH T32 GM008764). H.H.H. acknowledges support from Taiwan National Science and Technology Council (NSTC) Graduate Student Study Abroad Program (2022–2023) (111-2917-I-007-006). S.S. was supported by the American Heart Association under grant 20POST35210045. K.G. was supported in part by the National Institutes of Health from the NHLBI T32 Biology of the Lung training grant (NIH T32 HL007035).

AUTHOR CONTRIBUTIONS

Conceptualization, A.L. and C.S.C.; methodology, A.L., S.S., Y.C.T., and C.S.C.; investigation, A.L., H.H.H., K.G., S.K., and J.H.L.; writing – original draft, A.L.; writing – review & editing, A.L., S.S., Y.C.T., J.E., and C.S.C; visualization, A.L.; funding acquisition, C.S.C. and A.L.

DECLARATION OF INTERESTS

A provisional patent application has been filed by Boston University based on this work. C.S.C. is a founder and owns shares of Innolign Biomedical, a company that is developing engineered organ models for pharmaceutical research and development; Satellite Biosciences, a company that is developing cell-based therapies;

and Ropirio Therapeutics, a company developing molecular therapeutics for vascular disease.

Received: October 16, 2023
Revised: February 6, 2024
Accepted: April 1, 2024
Published: April 23, 2024

REFERENCES

1. Sherman, T.F. (1981). On connecting large vessels to small. The meaning of Murray's law. J. Gen. Physiol. *78*, 431–453. https://doi.org/10.1085/jgp.78.4.431.

2. Traore, M.A., and George, S.C. (2017). Tissue Engineering the Vascular Tree. Tissue Eng., Part B *23*, 505–514. https://doi.org/10.1089/ten.teb.2017.0010.

3. Kalogeris, T., Baines, C.P., Krenz, M., and Korthuis, R.J. (2012). Cell Biology of Ischemia/Reperfusion Injury. Int. Rev. Cell Mol. Biol. *298*, 229–317. https://doi.org/10.1016/B978-0-12-394309-5.00006-7.

4. Miller, J.S., Stevens, K.R., Yang, M.T., Baker, B.M., Nguyen, D.H.T., Cohen, D.M., Toro, E., Chen, A.A., Galie, P.A., Yu, X., et al. (2012). Rapid casting of patterned vascular networks for perfusable engineered three-dimensional tissues. Nat. Mater. *11*, 768–774. https://doi.org/10.1038/nmat3357.

5. Mirabella, T., Macarthur, J.W., Cheng, D., Ozaki, C.K., Woo, Y.J., Yang, M., and Chen, C.S. (2017). 3D-printed vascular networks direct therapeutic angiogenesis in ischaemia. Nat. Biomed. Eng. *1*, 0083. https://doi.org/10.1038/s41551-017-0083.

6. You, S., Xiang, Y., Hwang, H.H., Berry, D.B., Kiratitanaporn, W., Guan, J., Yao, E., Tang, M., Zhong, Z., Ma, X., et al. (2023). High cell density and high-resolution 3D bioprinting for fabricating vascularized tissues. Sci. Adv. *9*, eade7923. https://doi.org/10.1126/sciadv.ade7923.

7. Kolesky, D.B., Homan, K.A., Skylar-Scott, M.A., and Lewis, J.A. (2016). Three-dimensional bioprinting of thick vascularized tissues. Proc. Natl. Acad. Sci. USA *113*, 3179–3184. https://doi.org/10.1073/pnas.1521342113.

8. O'Connor, C., Brady, E., Zheng, Y., Moore, E., and Stevens, K.R. (2022). Engineering the multiscale complexity of vascular networks. Nat. Rev. Mater. *7*, 702–716. https://doi.org/10.1038/s41578-022-00447-8.

9. Skylar-Scott, M.A., Uzel, S.G.M., Nam, L.L., Ahrens, J.H., Truby, R.L., Damaraju, S., and Lewis, J.A. (2019). Biomanufacturing of organ-specific tissues with high cellular density and embedded vascular channels. Sci. Adv. *5*, eaaw2459. https://doi.org/10.1126/sciadv.aaw2459.

10. Kim, S., Lee, H., Chung, M., and Jeon, N.L. (2013). Engineering of functional, perfusable 3D microvascular networks on a chip. Lab Chip *13*, 1489–1500. https://doi.org/10.1039/c3lc41320a.

11. Kaully, T., Kaufman-Francis, K., Lesman, A., and Levenberg, S. (2009). Vascularization—The Conduit to Viable Engineered Tissues. Tissue Eng., Part B *15*, 159–169. https://doi.org/10.1089/ten.teb.2008.0193.

12. Szklanny, A.A., Machour, M., Redenski, I., Chochola, V., Goldfracht, I., Kaplan, B., Epshtein, M., Simaan Yameen, H., Merdler, U., Feinberg, A., et al. (2021). 3D Bioprinting of Engineered Tissue Flaps with Hierarchical Vessel Networks (VesselNet) for Direct Host-To-Implant Perfusion. Adv. Mater. *33*, 2102661. https://doi.org/10.1002/adma.202102661.

13. Song, H.H.G., Lammers, A., Sundaram, S., Rubio, L., Chen, A.X., Li, L., Eyckmans, J., Bhatia, S.N., and Chen, C.S. (2020). Transient Support from Fibroblasts is Sufficient to Drive Functional Vascularization in Engineered Tissues. Adv. Funct. Mater. *30*, 2003777. https://doi.org/10.1002/adfm.202003777.

14. Yao, R., Alkhawtani, A.Y.F., Chen, R., Luan, J., and Xu, M. (2019). Rapid and efficient in vivo angiogenesis directed by electro-assisted bioprinting of alginate/collagen microspheres with human umbilical vein endothelial cell coating layer. Int. J. Bioprinting *5*, 3–14. https://doi.org/10.18063/IJB.V5I2.194.

15. Yao, H., Hsieh, Y.P., Kong, J., and Hofmann, M. (2020). Modelling electrical conduction in nanostructure assemblies through complex networks. Nat. Mater. *19*, 745–751. https://doi.org/10.1038/s41563-020-0664-1.

16. Khan, T., Irfan, M.S., Ali, M., Dong, Y., Ramakrishna, S., and Umer, R. (2021). Insights to low electrical percolation thresholds of carbon-based polypropylene nanocomposites. Carbon *176*, 602–631. https://doi.org/10.1016/j.carbon.2021.01.158.

17. Kim, K.K., Hong, S., Cho, H.M., Lee, J., Suh, Y.D., Ham, J., and Ko, S.H. (2015). Highly Sensitive and Stretchable Multidimensional Strain Sensor with Prestrained Anisotropic Metal Nanowire Percolation Networks. Nano Lett. *15*, 5240–5247. https://doi.org/10.1021/acs.nanolett.5b01505.

18. Ge, D., Yang, L., Fan, L., Zhang, C., Xiao, X., Gogotsi, Y., and Yang, S. (2015). Foldable supercapacitors from triple networks of macroporous cellulose fibers, single-walled carbon nanotubes and polyaniline nanoribbons. Nano Energy *11*, 568–578. https://doi.org/10.1016/j.nanoen.2014.11.023.

19. Ding, P., Zhang, J., Song, N., Tang, S., Liu, Y., and Shi, L. (2015). Anisotropic thermal conductive properties of hot-pressed polystyrene/graphene composites in the through-plane and in-plane directions. Compos. Sci. Technol. *109*, 25–31. https://doi.org/10.1016/j.compscitech.2015.01.015.

20. Matsubara, H., and Ohara, T. (2021). Effect of the in-plane aspect ratio of a graphene filler on anisotropic heat conduction in paraffin/graphene composites. Phys. Chem. Chem. Phys. *23*, 12082–12092. https://doi.org/10.1039/D1CP00556A.

21. Milewski, J.V. (1978). The Combined Packing of Rods and Spheres in Reinforcing Plastics. Ind. Eng. Chem. Prod. Res. Dev. *17*, 363–366. https://doi.org/10.1021/i360068a016.

22. Caliari, S.R., and Harley, B.A.C. (2011). The effect of anisotropic collagen-GAG scaffolds and growth factor supplementation on tendon cell recruitment, alignment, and metabolic activity. Biomaterials *32*, 5330–5340. https://doi.org/10.1016/j.biomaterials.2011.04.021.

23. Sayers, C.M. (1990). Stress-induced fluid flow anisotropy in fractured rock. Transport Porous Media *5*, 287–297. https://doi.org/10.1007/BF00140017.

24. King, P., and Masihi, M. (2009). Percolation in Porous Media. In Complex Media and Percolation Theory, M. Sahimi and A.G. Hunt, eds. (Springer US), pp. 237–254. https://doi.org/10.1007/978-1-0716-1457-0_389.

25. Xu, W., and Jiao, Y. (2019). Theoretical framework for percolation threshold, tortuosity and transport properties of porous materials containing 3D non-spherical pores. Int. J. Eng. Sci. *134*, 31–46. https://doi.org/10.1016/j.ijengsci.2018.10.004.

26. Malthe-Sørenssen, A. (2020). Percolation Theory Using python (University of Oslo).

27. Stauffer, D., and Aharony, A. (2010). Introduction to Percolation Theory, 2nd ed. (Taylor & Francis).

28. Malthe-Sorenssen, A. (2015). Percolation and Disordered Systems-A Numerical Approach.

29. Nguyen, D.H.T., Stapleton, S.C., Yang, M.T., Cha, S.S., Choi, C.K., Galie, P.A., and Chen, C.S. (2013). Biomimetic model to reconstitute angiogenic sprouting morphogenesis in vitro. Proc. Natl. Acad. Sci. USA *110*, 6712–6717. https://doi.org/10.1073/pnas.1221526110.

30. Tien, J., and Dance, Y.W. (2021). Microfluidic Biomaterials. Adv. Healthcare Mater. *10*, 2001028. https://doi.org/10.1002/adhm.202001028.

31. Jakus, A.E., Secor, E.B., Rutz, A.L., Jordan, S.W., Hersam, M.C., and Shah, R.N. (2015). Three-Dimensional Printing of High-Content Graphene Scaffolds for Electronic and Biomedical Applications. ACS Nano *9*,

4636–4648. https://doi.org/10.1021/acsnano.5b01179.

32. Raney, J.R., and Lewis, J.A. (2015). Printing mesoscale architectures. MRS Bull. *40*, 943–950. https://doi.org/10.1557/mrs.2015.235.

33. Xing, R., Yang, J., Zhang, D., Gong, W., Neumann, T.V., Wang, M., Huang, R., Kong, J., Qi, W., and Dickey, M.D. (2023). Metallic gels for conductive 3D and 4D printing. Matter *6*, 2248–2262. https://doi.org/10.1016/j.matt.2023.06.015.

34. Cheung Shum, H., Varnell, J., and Weitz, D.A. (2012). Microfluidic fabrication of water-in-water (w/w) jets and emulsions. Biomicrofluidics *6*, 12808–128089. https://doi.org/10.1063/1.3670365.

35. Zhao, J., Xiong, W., Yu, N., and Yang, X. (2017). Continuous jetting of alginate microfiber in atmosphere based on a microfluidic chip. Micromachines *8*, 8. https://doi.org/10.3390/mi8010008.

36. Deng, X., Ren, Y., Hou, L., Liu, W., Jia, Y., and Jiang, H. (2018). Electric Field-Induced Cutting of Hydrogel Microfibers with Precise Length Control for Micromotors and Building Blocks. ACS Appl. Mater. Interfaces *10*, 40228–40237. https://doi.org/10.1021/acsami.8b12597.

37. Chaurasia, A.S., and Sajjadi, S. (2019). Transformable bubble-filled alginate microfibers via vertical microfluidics. Lab Chip *19*, 851–863. https://doi.org/10.1039/c8lc01081a.

38. Wang, Y., Hu, X., Kankala, R.K., Yang, D.-Y., Zhu, K., Wang, S.-B., Zhang, Y.S., and Chen, A.-Z. (2019). Endothelialized microrods for minimally invasive *in situ* neovascularization. Biofabrication *12*, 015011. https://doi.org/10.1088/1758-5090/ab47eb.

39. Saeki, K., Hiramatsu, H., Hori, A., Hirai, Y., Yamada, M., Utoh, R., and Seki, M. (2020). Sacrificial Alginate-Assisted Microfluidic Engineering of Cell-Supportive Protein Microfibers for Hydrogel-Based Cell Encapsulation. ACS Omega *5*, 21641–21650. https://doi.org/10.1021/acsomega.0c02385.

40. Xie, R., Liang, Z., Ai, Y., Zheng, W., Xiong, J., Xu, P., Liu, Y., Ding, M., Gao, J., Wang, J., and Liang, Q. (2021). Composable microfluidic spinning platforms for facile production of biomimetic perfusable hydrogel microtubes. Nat. Protoc. *16*, 937–964. https://doi.org/10.1038/s41596-020-00442-9.

41. Håti, A.G., Bassett, D.C., Ribe, J.M., Sikorski, P., Weitz, D.A., and Stokke, B.T. (2016). Versatile, cell and chip friendly method to gel alginate in microfluidic devices. Lab Chip *16*, 3718–3727. https://doi.org/10.1039/c6lc00769d.

42. Duraj-Thatte, A.M., Manjula-Basavanna, A., Rutledge, J., Xia, J., Hassan, S., Sourlis, A., Rubio, A.G., Lesha, A., Zenkl, M., Kan, A., et al. (2021). Programmable microbial ink for 3D printing of living materials produced from genetically engineered protein nanofibers. Nat. Commun. *12*, 6600. https://doi.org/10.1038/s41467-021-26791-x.

43. Wang, Y., Yin, R., Jin, L., Liu, M., Gao, Y., Raney, J., and Yang, S. (2023). 3D-Printed Photoresponsive Liquid Crystal Elastomer Composites for Free-Form Actuation. Adv. Funct. Mater. *33*, 2210614. https://doi.org/10.1002/adfm.202210614.

44. Xu, W., Su, X., and Jiao, Y. (2016). Continuum percolation of congruent overlapping spherocylinders. Phys. Rev. E *94*, 032122. https://doi.org/10.1103/PhysRevE.94.032122.

45. Rudolph, A.M. (1983). Hepatic and Ductus Venosus Blood Flows During Fetal Life. Hepatology *3*, 254–258. https://doi.org/10.1002/hep.1840030220.

46. Wacker, C.M., Wiesmann, F., Bock, M., Jakob, P., Sandstede, J.J.W., Lehning, A., Ertl, G., Schad, L.R., Haase, A., and Bauer, W.R. (2002). Determination of regional blood volume and intra- extracapillary water exchange in human myocardium using feruglose: First clinical results in patients with coronary artery disease. Magn. Reson. Med. *47*, 1013–1016. https://doi.org/10.1002/mrm.10125.

47. Wang, H., Golob, E.J., and Su, M.-Y. (2006). Vascular volume and blood-brain barrier permeability measured by dynamic contrast enhanced MRI in hippocampus and cerebellum of patients with MCI and normal controls. J. Magn. Reson. Imag. *24*, 695–700. https://doi.org/10.1002/jmri.20669.

48. Jafarnejad, M., Ismail, A.Z., Duarte, D., Vyas, C., Ghahramani, A., Zawieja, D.C., Lo Celso, C., Poologasundarampillai, G., and Moore, J.E. (2019). Quantification of the Whole Lymph Node Vasculature Based on Tomography of the Vessel Corrosion Casts. Sci. Rep. *9*, 13380. https://doi.org/10.1038/s41598-019-49055-7.

49. Bland, E., Dréau, D., and Burg, K.J.L. (2013). Overcoming hypoxia to improve tissue-engineering approaches to regenerative medicine: Tissue-engineering hypoxia and preconditioning. J. Tissue Eng. Regen. Med. *7*, 505–514. https://doi.org/10.1002/term.540.

50. Erapaneedi, R., Belousov, V.V., Schäfers, M., and Kiefer, F. (2016). A novel family of fluorescent hypoxia sensors reveal strong heterogeneity in tumor hypoxia at the cellular level. EMBO J. *35*, 102–113. https://doi.org/10.15252/embj.201592775.

51. Sattiraju, A., Kang, S., Giotti, B., Chen, Z., Marallano, V.J., Brusco, C., Ramakrishnan, A., Shen, L., Tsankov, A.M., Hambardzumyan, D., et al. (2023). Hypoxic niches attract and sequester tumor-associated macrophages and cytotoxic T cells and reprogram them for immunosuppression. Immunity *56*, 1825–1843.e6. https://doi.org/10.1016/j.immuni.2023.06.017.

52. Nolan, C., Hall, L.S., Barlow, G.H., and Tribby, I.I. (1977). Plasminogen activator from human embryonic kidney cell cultures. Biochim. Biophys. Acta *496*, 384–400. https://doi.org/10.1016/0304-4165(77)90321-X.

53. Collen, D. (1987). Molecular mechanisms of fibrinolysis and their application to fibrin-specific thrombolytic therapy. J. Cell. Biochem. *33*, 77–86. https://doi.org/10.1002/jcb.240330202.

54. Gjorevski, N., and Nelson, C.M. (2011). Integrated morphodynamic signalling of the mammary gland. Nat. Rev. Mol. Cell Biol. *12*, 581–593. https://doi.org/10.1038/nrm3168.

55. Griffith, C.K., Miller, C., Sainson, R.C.A., Calvert, J.W., Jeon, N.L., Hughes, C.C.W., and George, S.C. (2005). Diffusion limits of an in vitro thick prevascularized tissue. Tissue Eng. *11*, 257–266. https://doi.org/10.1089/ten.2005.11.257.

56. Kolesky, D.B., Truby, R.L., Gladman, A.S., Busbee, T.A., Homan, K.A., and Lewis, J.A. (2014). 3D bioprinting of vascularized, heterogeneous cell-laden tissue constructs. Adv. Mater. *26*, 3124–3130. https://doi.org/10.1002/adma.201305506.

57. Machour, M., Hen, N., Goldfracht, I., Safina, D., Davidovich-Pinhas, M., Bianco-Peled, H., and Levenberg, S. (2022). Print-and-Grow within a Novel Support Material for 3D Bioprinting and Post-Printing Tissue Growth. Adv. Sci. *9*, 2200882. https://doi.org/10.1002/advs.202200882.

58. Mora-Boza, A., Mulero-Russe, A., Caprio, N.D., Burdick, J.A., Singh, A., and García, A.J. (2023). Facile Photopatterning of Perfusable Microchannels in Synthetic Hydrogels to Recreate Microphysiological Environments. Adv. Mater. *35*, e2306765. https://doi.org/10.1002/adma.202306765.

59. Pradhan, S., Keller, K.A., Sperduto, J.L., and Slater, J.H. (2017). Fundamentals of Laser-Based Hydrogel Degradation and Applications in Cell and Tissue Engineering. Adv. Healthcare Mater. *6*, 1–28. https://doi.org/10.1002/adhm.201700681.

60. Mokhena, T.C., Mochane, M.J., Mtibe, A., John, M.J., Sadiku, E.R., and Sefadi, J.S. (2020). Electrospun Alginate Nanofibers Toward Various Applications: A Review. Materials *13*, 934. https://doi.org/10.3390/ma13040934.

61. Palikuqi, B., Nguyen, D.H.T., Li, G., Schreiner, R., Pellegata, A.F., Liu, Y., Redmond, D., Geng, F., Lin, Y., Gómez-Salinero, J.M., et al. (2020). Adaptable haemodynamic endothelial cells for organogenesis and tumorigenesis. Nature *585*, 426–432. https://doi.org/10.1038/s41586-020-2712-z.

62. Zohar, B., Debbi, L., Machour, M., Nachum, N., Redenski, I., Epshtein, M., Korin, N., and Levenberg, S. (2023). A micro-channel array in a tissue engineered vessel graft guides vascular morphogenesis for anastomosis with self-assembled vascular networks. Acta Biomater. *163*, 182–193. https://doi.org/10.1016/j.actbio.2022.05.026.

63. Weaver, J.D., Headen, D.M., Hunckler, M.D., Coronel, M.M., Stabler, C.L., and García, A.J. (2018). Design of a vascularized synthetic poly(ethylene glycol) macroencapsulation device for islet transplantation. Biomaterials *172*, 54–65. https://doi.org/10.1016/j.biomaterials.2018.04.047.

64. Lee, J.B., Kim, D.-H., Yoon, J.-K., Park, D.B., Kim, H.-S., Shin, Y.M., Baek, W., Kang, M.-L., Kim, H.J., and Sung, H.-J. (2020). Microchannel network hydrogel induced ischemic blood perfusion connection. Nat. Commun. *11*, 615. https://doi.org/10.1038/s41467-020-14480-0.

65. (2006). HEPES-buffered saline. Cold Spring Harb. Protoc. *2006*, pdb.rec8786. https://doi.org/10.1101/pdb.rec8786.

66. Litvinov, R.I., and Weisel, J.W. (2017). Fibrin mechanical properties and their structural origins. Matrix Biol. *60–61*, 110–123. https://doi.org/10.1016/j.matbio.2016.08.003.

67. Doyle, A.D. (2016). Generation of 3D Collagen Gels with Controlled Diverse Architectures. CP Cell Biology *72*, 10.20.1–10.20.16. https://doi.org/10.1002/cpcb.9.

68. Toepfer, C.N., Garfinkel, A.C., Venturini, G., Wakimoto, H., Repetti, G., Alamo, L., Sharma, A., Agarwal, R., Ewoldt, J.K., Cloonan, P., et al. (2020). Myosin Sequestration Regulates Sarcomere Function, Cardiomyocyte Energetics, and Metabolism, Informing the Pathogenesis of Hypertrophic Cardiomyopathy. Circulation *141*, 828–842. https://doi.org/10.1161/CIRCULATIONAHA.119.042339.

69. Zhang, K., Cloonan, P.E., Sundaram, S., Liu, F., Das, S.L., Ewoldt, J.K., Bays, J.L., Tomp, S., Toepfer, C.N., Marsiglia, J.D.C., et al. (2021). Plakophilin-2 truncating variants impair cardiac contractility by disrupting sarcomere stability and organization. Sci. Adv. *7*, eabh3995. https://doi.org/10.1126/sciadv.abh3995.

70. Hsu, H.-H., Ko, P.-L., Peng, C.-C., Cheng, Y.-J., Wu, H.-M., and Tung, Y.-C. (2023). Studying sprouting angiogenesis under combination of oxygen gradients and co-culture of fibroblasts using microfluidic cell culture model. Mater. Today. Bio *21*, 100703. https://doi.org/10.1016/j.mtbio.2023.100703.

71. Wu, H.-M., Lee, T.-A., Ko, P.-L., Liao, W.-H., Hsieh, T.-H., and Tung, Y.-C. (2019). Widefield frequency domain fluorescence lifetime imaging microscopy (FD-FLIM) for accurate measurement of oxygen gradients within microfluidic devices. Analyst *144*, 3494–3504. https://doi.org/10.1039/C9AN00143C.

72. Rueden, C.T., Schindelin, J., Hiner, M.C., DeZonia, B.E., Walter, A.E., Arena, E.T., and Eliceiri, K.W. (2017). ImageJ2: ImageJ for the next generation of scientific image data. BMC Bioinf. *18*, 529. https://doi.org/10.1186/s12859-017-1934-z.

73. Huang, L.-K., and Wang, M.-J.J. (1995). Image thresholding by minimizing the measures of fuzziness. Pattern Recogn. *28*, 41–51. https://doi.org/10.1016/0031-3203(94)E0043-K.